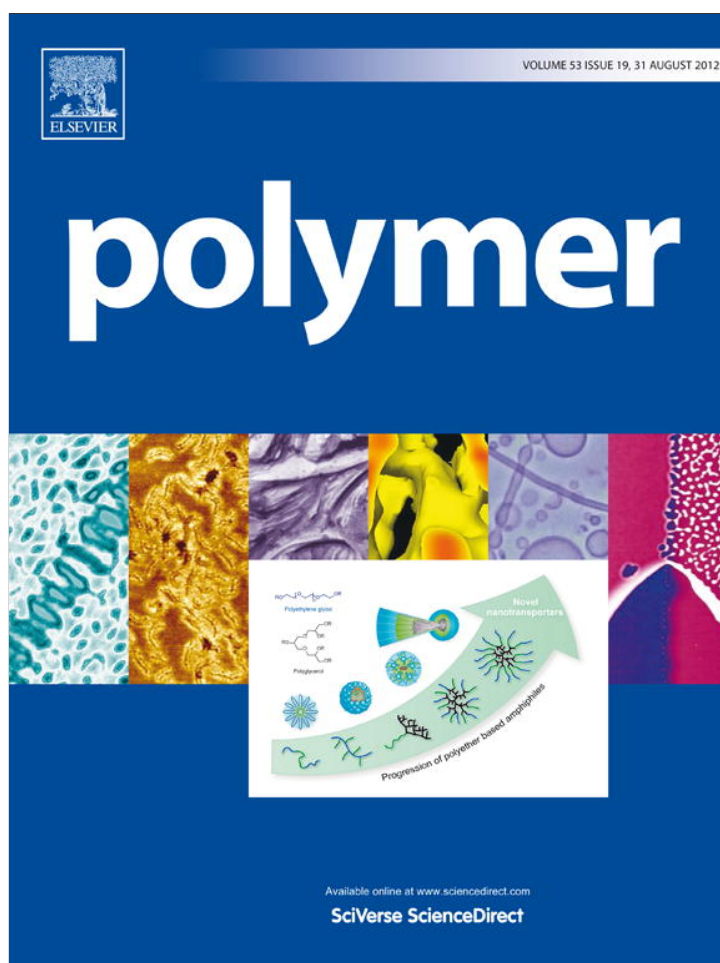


Provided for non-commercial research and education use.
Not for reproduction, distribution or commercial use.



This article appeared in a journal published by Elsevier. The attached copy is furnished to the author for internal non-commercial research and education use, including for instruction at the authors institution and sharing with colleagues.

Other uses, including reproduction and distribution, or selling or licensing copies, or posting to personal, institutional or third party websites are prohibited.

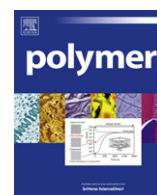
In most cases authors are permitted to post their version of the article (e.g. in Word or Tex form) to their personal website or institutional repository. Authors requiring further information regarding Elsevier's archiving and manuscript policies are encouraged to visit:

<http://www.elsevier.com/copyright>



Contents lists available at SciVerse ScienceDirect

Polymer

journal homepage: www.elsevier.com/locate/polymer

Electrically bistable digital memory behaviors of thin films of polyimides based on conjugated bis(triphenylamine) derivatives

Kyungtae Kim^{a,1}, Hung-Ju Yen^{b,1}, Yong-Gi Ko^a, Cha-Wen Chang^b, Wonsang Kwon^a, Guey-Sheng Liou^{b,**}, Moonhor Ree^{a,*}

^a Department of Chemistry, Division of Advanced Materials Science, Center for Electro-Photo Behaviors in Advanced Molecular Systems, Pohang Accelerator Laboratory, Polymer Research Institute, and BK School of Molecular Science, Pohang University of Science & Technology, Pohang 790-784, Republic of Korea

^b Institute of Polymer Science and Engineering, National Taiwan University, Taipei 10617, Taiwan, ROC

ARTICLE INFO

Article history:

Received 12 April 2012

Received in revised form

9 July 2012

Accepted 14 July 2012

Available online 20 July 2012

Keywords:

High temperature aromatic polyimide

Bis(triphenylamine) derivatives

Nonvolatile memory

ABSTRACT

Three functional polyimides (PIs) bearing conjugated bis(triphenylamine) (2TPA) derivatives with electron-donating and accepting groups were synthesized with reasonably high molecular weights. The PIs exhibited high thermal and dimensional stabilities and furthermore produced high-quality nanoscale thin films via conventional solution coating process. All of the PIs in the films were found to be amorphous, but they were oriented somewhat preferentially in the film plane, rather than randomly. Their film densities and interchain distances were measured, and the optical and electrochemical properties were determined. All of the PIs in the devices with aluminum top and bottom electrodes initially revealed a high resistance (OFF-state). However, under positive and negative voltage sweeps, the PIs demonstrated volatile or nonvolatile digital memory behavior, depending on the substituents of the 2TPA unit. The 2TPA-based PI, as well as the PI bearing 2TPA with electron-donating methoxy substituents showed unipolar write-once-read-many-times (WORM) memory behavior, whereas the 2TPA-based PI containing electron-accepting cyano groups exhibited unipolar dynamic random access memory (DRAM) behavior. All of the PI films revealed excellent retention abilities in both the OFF- and ON-state, even under ambient air conditions. Moreover, they all revealed high ON/OFF current ratios (10^6 – 10^{10}). All of the memory behaviors were found to be governed by a mechanism involving trap-limited space-charge limited conduction and local filament formation. Such memory behaviors were further investigated in detail with taking into consideration the PI components' chemical nature and molecular orbital levels, possible trapping sites, substituents' effect, and the metal electrodes' work function. Overall, this study demonstrated that the thermally, dimensionally stable PIs are highly suitable for the low-cost mass production of high performance, polarity-free digital memory devices that can be operated with very low power consumption. Moreover, the memory mode can be tuned by changing the substituent in the 2TPA unit.

© 2012 Elsevier Ltd. All rights reserved.

1. Introduction

In general, polymers can be easily processable in various ways, including conventional solution coating and melt molding, and their structures and properties can be tailored through chemical synthesis. Furthermore, polymers can be easily incorporated into a highly dense multilayer structure of advanced memory devices,

which are currently demanded for the storage of multimedia data, such as videos [1–5].

In particular, aromatic polyimides (PIs) are known to possess excellent thermal stability, dimensional stability, and mechanical properties [6–10]. Due to these advantageous properties, much effort has recently been made to develop high performance PI materials for advanced memory devices [11–18]. As a result, several PIs were reported for the fabrication of memory devices [11–18]. They revealed various memory behaviors (i.e., switchable, permanent and volatile memories) with unipolarity or bipolarity, depending on the chemical structure as well as the film thickness. Poly(4,4'-amino-triphenylene hexafluoroisopropylidenediphthalimide) (6F-TPA PI) was reported to exhibit dynamic random access memory (DRAM)

* Corresponding author. Tel.: +82 54 279 2120; fax: +82 54 279 3399.

** Corresponding author. Tel.: +886 2 3336 5315; fax: +886 2 3336 5237.

E-mail addresses: gслиou@ntu.edu.tw (G.-S. Liou), ree@postech.edu (M. Ree).

¹ K. Kim and H.-J. Yen contributed equally to this work.

behavior with polarity [11]. Compared to 6F-TPA PI, poly(4,4'-amino(4-hydroxyphenyl)diphenylene hexafluoroisopropylidene diphthalimide) additionally possessed only one hydroxyl group per TPA unit, but interestingly revealed unipolar write-once-read-many-times (WORM) memory behavior [12], which was quite different from the bipolar DRAM behavior observed for 6F-TPA PI. Furthermore, poly(*N,N,N'*-diphenyl-*N'*-1,4-phenyl)-*N,N*-4,4'-diphenylene hexafluoroisopropylidenediphthalimide) (6F-2TPA PI) revealed volatile DRAM behavior with polarity and nonvolatile WORM memory characteristics with and without polarity depending on the

thickness [13]; namely, the 100 nm thick films showed DRAM behavior while the films with a thickness of 15 nm to 100 nm exhibited WORM behavior. Poly(3,3'-di(4-(diphenylamino)benzylidene)-iminoethoxy)-4,4'-biphenylene hexafluoroisopropylidenediphthalimide) demonstrated unipolar and bipolar nonvolatile switching behaviors [14]. Poly(3,3'-bis(diphenylcarbamyloxy)-4,4'-biphenylene hexafluoroisopropylidenediphthalimide) was found to exhibit rewritable nonvolatile memory characteristics [15]. On the other hand, poly(3,3'-bis(*N*-ethylenyloxy)carbazole)-4,4'-biphenylene hexafluoroisopropylidenediphthalimide), a polyimide containing carbazole moieties, demonstrated rewritable unipolar nonvolatile memory behavior [16]. In contrast, other aromatic polyimides containing carbazole moieties (which were synthesized from 3,3'-bis[9-carbazole(ethyloxy)biphenyl]-4,4'-diamine) exhibited unipolar WORM memory behaviors, regardless of the dianhydride units in the polymer backbone [17]. Poly(3,3'-di(9-anthracenemethoxy)-4,4'-biphenylene hexafluoroisopropylidenediphthalimide), a polyimide containing anthracene moieties, revealed rewritable unipolar and bipolar nonvolatile memory behaviors [18]. Overall, the development of high-performance PIs for memory devices still remains in its early stages. Furthermore, to facilitate the development of high performance memory PIs, it is essential to understand the relationship between their electrical memory behavior and their chemical structure.

In this study, we synthesized three aromatic PIs bearing bis(tripheylamine) (2TPA) derivatives with electron-accepting and donating groups, and investigated their electrical memory behaviors: poly(*N,N*-bis(4-aminophenyl)-*N,N'*-diphenyl-1,4-phenylene 3,3',4,4'-diphenylsulfonyltetracarboximide) (DSDA-2TPA PI), poly(*N,N*-bis(4-aminophenyl)-*N,N'*-di(4-methoxyphenyl)-1,4-phenylene 3,3',4,4'-diphenylsulfonyltetracarboximide) (DSDA-2TPA-OMe₂ PI), and poly(*N,N*-bis(4-aminophenyl)-*N,N'*-di(4-cyanophenyl)-

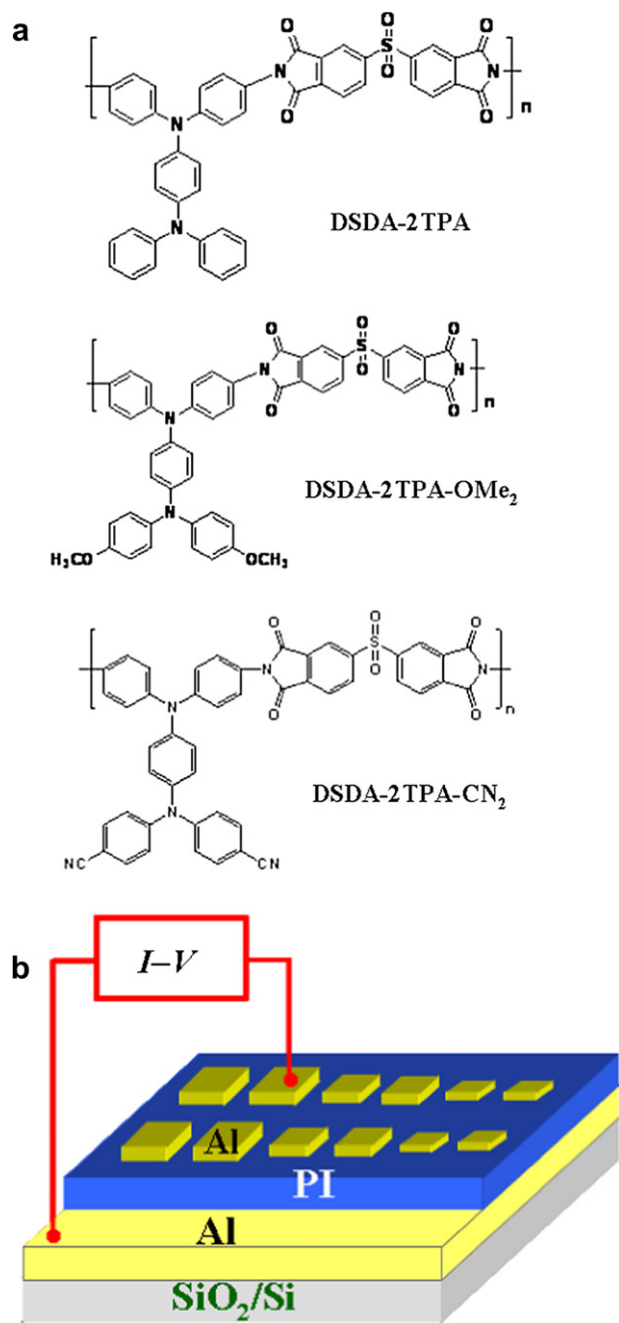


Fig. 1. (a) Chemical structures of aromatic polyimides bearing bis(tripheylamine) (2TPA) derivatives with electron-donating and accepting groups: DSDA-2TPA PI, DSDA-2TPA-OMe₂ PI, and DSDA-2TPA-CN₂ PI. (b) A schematic diagram of the memory devices fabricated with nanoscale thin films of the PIs and aluminum (Al) top and bottom electrodes.

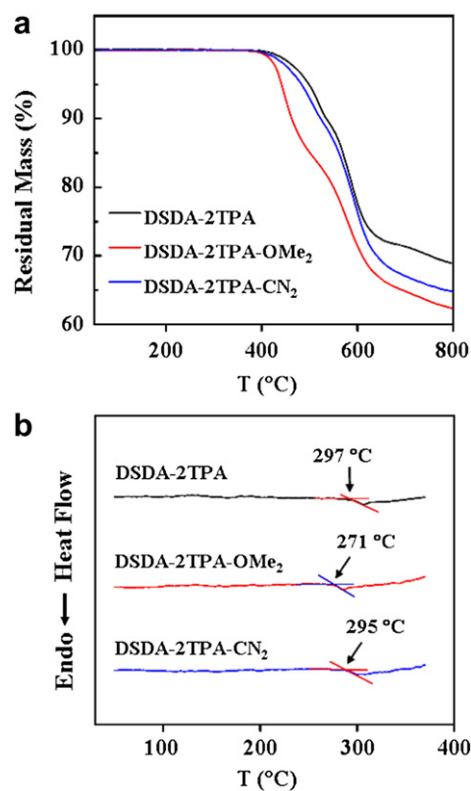


Fig. 2. (a) TGA and (b) DSC thermograms of the PI polymers, which were measured at a rate of 10.0 °C/min under nitrogen atmosphere.

1,4-phenylene 3,3',4,4'-diphenylsulfonyltetracarboximide (DSDA-2TPA-CN₂ PI) (Fig. 1a). The PIs exhibited high thermal and dimensional stability, and produced high quality nanoscale thin films via conventional solution coating and drying process. These PIs were found to reveal write-once-read-many-times (WORM) memory and dynamic random access memory (DRAM) behaviors without polarity, depending on the 2TPA derivatives. The observed memory characteristics were understood with taking into consideration the chemical nature including substituents, morphological structure and interface, and optical and electrochemical properties, as well as the work functions of metal electrodes. In addition, their switching mechanism was investigated.

2. Experimental

DSPA-2TPA PI was synthesized in *N*-methyl-2-pyrrolidinone (NMP) from 3,3',4,4'-diphenylsulfonyltetracarboxylic dianhydride (DSDA) and *N,N*-bis(4-aminophenyl)-*N',N'*-diphenyl-1,4-phenylene diamine (2TPA) as described in the literature [19]. In similar synthetic manner, DSDA-2TPA-OMe₂ PI and DSDA-2TPA-CN₂ PI were prepared from the polymerizations of DSDA with *N,N*-bis(4-

aminophenyl)-*N',N'*-di(4-methoxyphenyl)-1,4-phenylene diamine (2TPA-OMe₂) and *N,N*-bis(4-aminophenyl)-*N',N'*-di(4-cyanophenyl)-1,4-phenylene diamine (2TPA-CN₂) respectively.

For the obtained PIs, inherent viscosities were determined with a concentration of 0.5 g/dL in NMP at 30 °C using a Tamson TV-2000 viscometer. Furthermore, for some selected PIs, molecular weights were measured at 70 °C using a gel permeation chromatography (GPC) system (Lab Alliance RI2000 Instruments) connected with a refractive index detector (Schambeck SFD GmbH). The GPC system was calibrated with polystyrene standards; *N,N*-dimethylformamide (DMF) was used with a flow rate of 1 mL/min as the eluent. Thermal properties were measured in nitrogen atmosphere using a thermogravimetric analyzer (model TG/DTA-6300, Seiko) and a differential scanning calorimeter (model DSC 220CU, Seiko); dry nitrogen gas was purged at a flow rate of 100 cc/min and a ramping rate of 10.0 °C/min were employed.

Aluminum (Al) bottom electrodes with a thickness of 300 nm were prepared onto pre-cleaned silicon (Si) substrates by electron-beam deposition. Homogenous solutions of the three PIs were prepared by dissolving the polymers (1 wt%) in cyclopentanone. The resulting solutions were filtered through PTFE-membrane

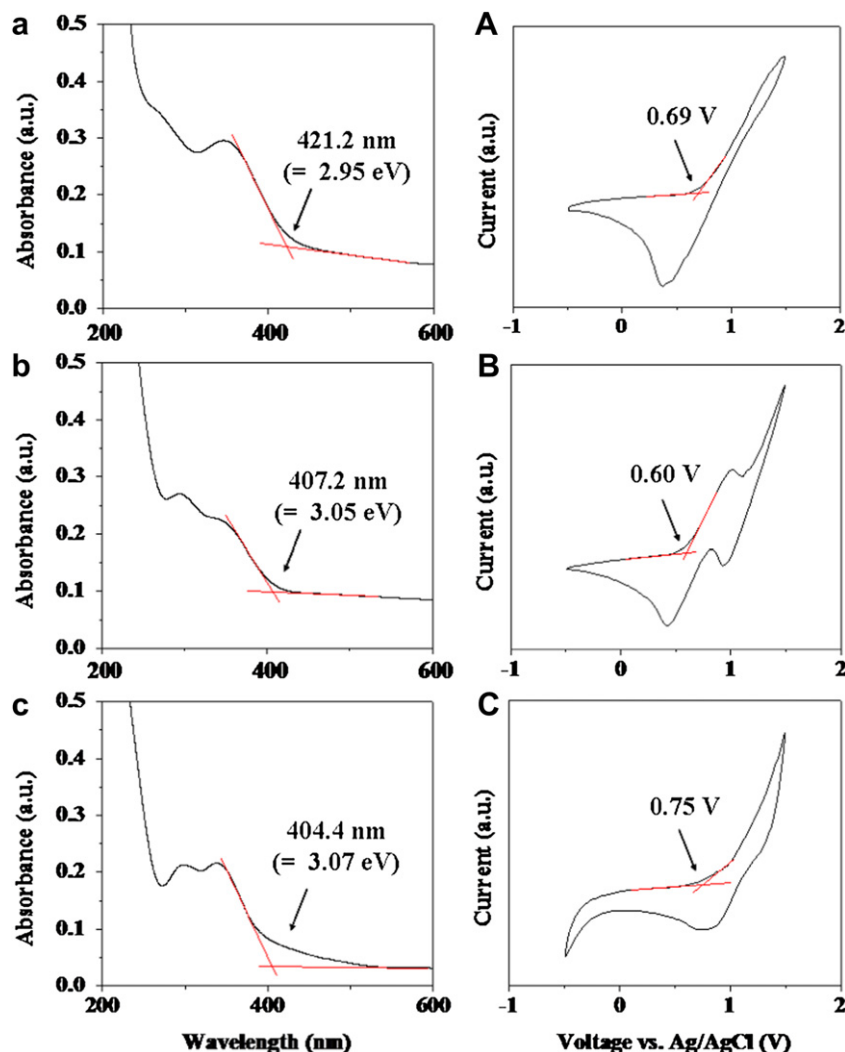


Fig. 3. UV-vis spectra and CV responses of the PIs films, which were coated on quartz substrates and fabricated with Au electrodes supported by silicon substrates respectively: (a,A) DSDA-2TPA PI; (b,B) DSDA-2TPA-OMe₂ PI; (c,C) DSDA-2TPA-CN₂ PI. The CV measurements were carried out in aqueous 0.1 M tetrabutylammonium tetrafluoroborate in acetonitrile using an electrochemical workstation (IM6ex impedance analyzer) with a platinum gauze counter electrode and an Ag/AgCl (3.8 M KCl) reference electrode. A scan rate of 100 mV/s was used.

microfilters with a pore size of 1.0 μm . The polymer solutions were spin-coated onto the electrodes and Si substrates at 2000 rpm for 60 s. The films were then baked at 80 $^{\circ}\text{C}$ for 24 h in vacuum. The thicknesses of the PI films were determined using a spectroscopic ellipsometer (model M2000, Woollam). Al top electrodes were thermally evaporated onto the polymer films at a pressure of $\sim 10^{-6}$ torr through a shadow mask. The top electrodes had a thickness of 300 nm and their area varied from 2.0 mm \times 2.0 mm to 0.5 mm \times 0.5 mm.

For X-ray reflectivity (XR) experiments, we prepared three kinds of samples for each polymer: (i) 30 nm thick PI films on Si substrates with native oxide layer; (ii) 30 nm thick PI films on the 10 nm thick Al electrodes which were deposited on Si substrates by electron-beam sputtering; (iii) thermally evaporated 10 nm thick Al electrodes on the 30 nm thick PI films coated onto Si substrates. Synchrotron XR measurements were performed at the 3C2 and 8C1 POSCO beamlines of the Pohang Accelerator Laboratory (PAL) [20]. A Si(111) double-crystal monochromator was used to select a wavelength λ of 0.1541 nm within an energy resolution of $\Delta\lambda/\lambda = 5 \times 10^{-4}$, and a Sagittal bender for the second crystal was used to focus the X-ray beam in the horizontal direction. The primary beam was defined by four slits before the sample, and another two slits were used as receiving slits after the sample. The beam was collimated at the sample position to 2 mm (horizontal) by 0.1 mm (vertical). The measured reflected intensity was normalized to the intensity of the primary beam, which was monitored with an ionization chamber. Specular reflection was measured in θ - 2θ scanning mode. The reflectivity R , i.e. the ratio of the reflected beam intensity to the primary beam intensity, was measured down to just above 10^{-8} . To obtain accurate determinations of the critical angles of the silicon substrate and of the thin film, 2θ was scanned at small increments of 0.01° at angles smaller than 1.0° . At higher angles the step width was increased to 0.02 – 0.1° . The obtained data were undergone data binning, geometrical correction, and background subtraction procedure described in literature [20,21].

Grazing-incidence X-ray scattering (GIXS) measurement was performed at the PAL 3C beamline [22,23]. Measurements were performed at a sample-to-detector distance (SDD) of 125 mm for grazing incidence wide-angle X-ray scattering (GIWAXS) and 2220 mm for grazing incidence small-angle X-ray scattering (GISAXS). Scattering data were typically collected for 30 s using X-ray radiation source of $\lambda = 0.138$ nm with a two-dimensional (2D) charge-coupled detector (CCD) (Roper Scientific, Trenton, NJ, USA). The incidence angle α_i of the X-ray beam was set at 0.183° for GIWAXS and 0.160° for GISAXS, respectively, which are between the critical angles of the PI film and the silicon substrate ($\alpha_{c,f}$ and $\alpha_{c,s}$). Scattering angles were corrected according to the positions of the X-ray beams reflected from the silicon substrate with respect to a pre-calibrated silver behenate (TCI, Japan) powder. Aluminum foil pieces were applied as a semitransparent beam stop because the intensity of the specular reflection from the substrate was much stronger than the scattering intensity of the polymer films near the critical angle.

Current–voltage (I - V) characteristics of the device were tested in air ambient condition using a Keithley 4200 semiconductor analyzer. I - V curves were recorded by performing forward and reverse voltage scans between -6.0 V and $+6.0$ V at a scan rate of 500 mV/s. Optical properties were measured with a Scinco ultraviolet–visible (UV–vis) spectrometer (model S-3100). Cyclic voltammetry (CV) measurements were carried out in an 0.1 M solution of tetrabutylammonium tetrafluoroborate in acetonitrile by using an electrochemical workstation (IM6ex impedance analyzer) with a platinum gauze counter electrode and an Ag/AgCl (saturated KCl) reference electrode, and polymers were coated onto the Au bottom electrode, which was deposited on a silicon wafer. A scan rate of 100 mV/s was used.

3. Results and discussion

The inherent viscosity η_{inh} was measured to be 0.72 dL/g for DSDA-2TPA PI, 0.64 dL/g for DSDA-2TPA-OMe₂ PI, and 0.99 dL/g for DSDA-2TPA-CN₂ PI. For some of the PIs, the weight average molecular weight (\overline{M}_w) and polydispersity index (PDI) were further determined by GPC analysis. The \overline{M}_w and PDI were 64,000 and 1.40 for DSDA-2TPA PI, and 80,000 and 1.47 for DSDA-2TPA-OMe₂ PI.

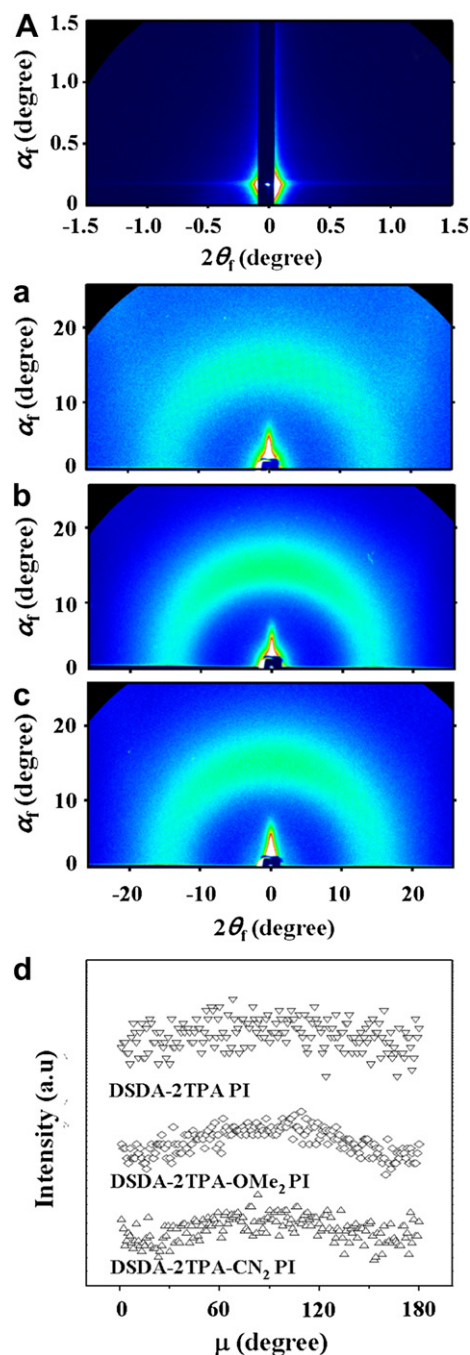


Fig. 4. Representative synchrotron 2D GIXS data pattern measured at 25 $^{\circ}\text{C}$ for the PI films (40 nm thick) deposited on silicon substrates: (A) GISAXS pattern of DSDA-2TPA PI; (a) GIWAXS pattern of DSDA-2TPA PI; (b) GIWAXS pattern of DSDA-2TPA-OMe₂ PI; (c) GIWAXS pattern of DSDA-2TPA-CN₂ PI; (d) azimuthal scattering profiles extracted along the amorphous halo ring from the GIWAXS patterns in (a)–(c). The GISAXS pattern was measured at 25 $^{\circ}\text{C}$ with $\alpha_i = 0.159^{\circ}$, whereas the GIWAXS patterns were measured with $\alpha_i = 0.187^{\circ}$.

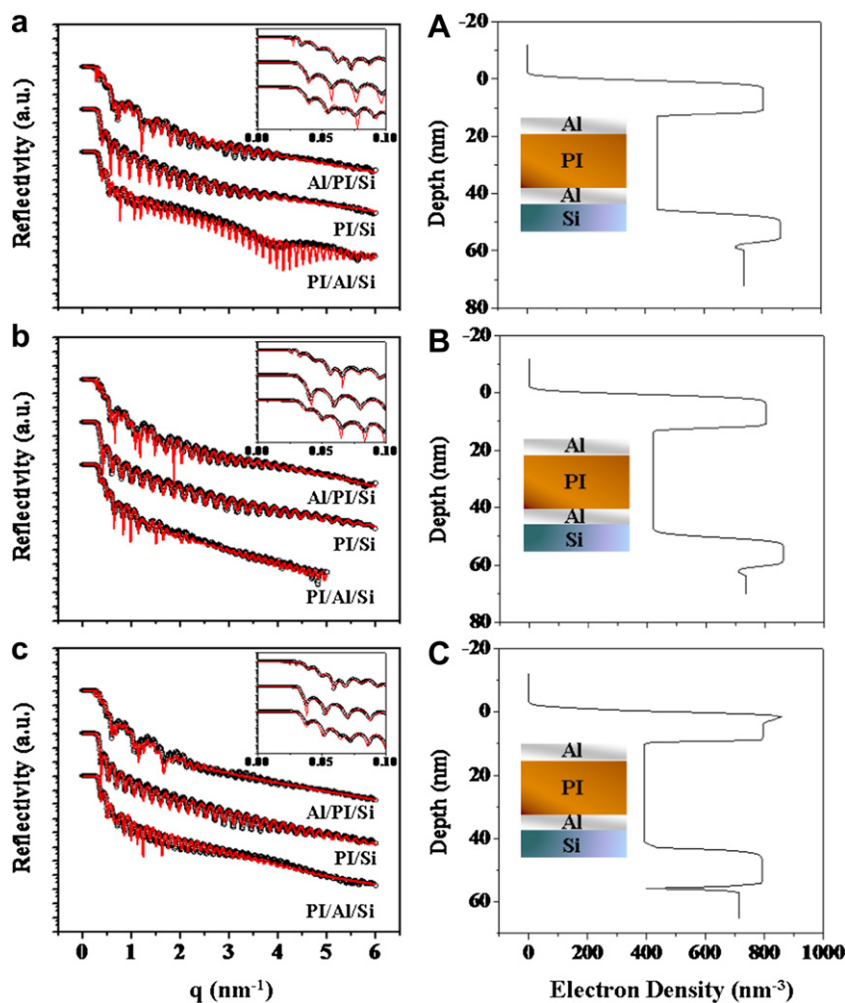


Fig. 5. Representative synchrotron XR profiles and electron density profiles of the PI thin films in contact with Si substrate, and Al bottom and top electrodes: (a,A) DSDA-2TPA PI; (b,B) DSDA-2TPA-OMe₂ PI; (c,C) DSDA-2TPA-CN₂ PI. The measured data (symbols) are represented with fitting curves (solid lines). Inset is the measured and fitted data enlarged in low angle region. Here the electron density profiles of Si/Al/PI/Al structures were made by the combination of the electron density profiles determined from the analysis of the XR profiles in (a)–(c).

Overall, all of the PIs were synthesized with reasonably high molecular weights. The onset temperature of degradation (T_d) was measured in nitrogen atmosphere to be 397 °C for DSDA-2TPA PI, 368 °C for DSDA-2TPA-OMe₂ PI, and 382 °C for DSDA-2TPA-CN₂ PI

(Fig. 2a). The onset temperature of glass transition (T_g) was measured to be 295 °C for DSDA-2TPA PI, 271 °C for DSDA-2TPA-OMe₂ PI, and 297 °C for DSDA-2TPA-CN₂ PI (Fig. 2b). Overall, the thermal and dimensional stabilities are comparable to those of

Table 1

Structural parameters and electron density profiles of various bilayer samples prepared from the PI films, silicon substrates, and Al electrodes.

Sample (top/bottom)	Bottom layer			PI layer			Top layer			Interlayer ^d		
	d^a (nm)	ρ_e^b (nm ⁻³)	σ^c (nm)	d^a (nm)	ρ_e^b (nm ⁻³)	σ^c (nm)	d^a (nm)	ρ_e^b (nm ⁻³)	σ^c (nm)	d^a (nm)	ρ_e^b (nm ⁻³)	σ^c (nm)
DSDA-2TPA PI												
PI/Si	–	778.2	0.3	30.2	443.2	0.2				0.6	670.7	0.4
PI/Al	12.2	793.1	1.4	31.7	438.6	0.4				1.4	886.8	0.4
Al/PI				34.2	444.6	0.2	10.2	803.1	1.0	1.9	471.3	1.0
DSDA-2TPA-OMe ₂ PI												
PI/Si	–	737.4	0.2	28.7	434.0	0.2				0.5	671.0	0.3
PI/Al	10.5	862.7	1.0	36.1	432.9	0.4				2.4	700.9	0.7
Al/PI				34.2	439.0	0.5	11.2	803.1	0.8	1.1	407.7	0.8
DSDA-2TPA-CN ₂ PI												
PI/Si	–	728.5	0.1	33.6	436.8	0.3				0.5	673.9	0.3
PI/Al	12.2	793.1	1.0	35.2	438.6	0.5				0.9	1109.3	0.4
Al/PI				41.2	428.7	0.2	11.5	829.3	0.9	1.0	530.5	1.1

^a Layer thickness.

^b Electron density of layer.

^c Roughness of layer in contact with air, lower or upper layer.

^d Silicon oxide layer for Si (bottom)/PI (top), aluminum oxide layer for Al/PI, and, PI-Al mixed layer (which is due to the roughness of interface) for PI/Al systems.

conventional aromatic PIs. The thermal property analysis found that the T_d of DSDA-2TPA PI was reduced by the incorporation of methoxy and cyano group. The T_g of DSDA-2TPA PI was slightly increased by the incorporation cyano group and, however, reduced by the incorporation of methoxy group.

Fig. 3a–c show the UV–vis absorption spectra of the PIs in thin films. From the spectra, the band gap (which is the difference between the highest occupied molecular orbital (HOMO) level and the lowest unoccupied molecular orbital (LUMO) level) was determined to be 2.95 eV for DSDA-2TPA PI, 3.05 eV for DSDA-2TPA-OMe₂ PI, and 3.07 eV for DSDA-TPA-CN₂ PI. Fig. 3A–C display the CV data of the PIs. The oxidation half-wave potentials ($E_{1/2}$) vs. Ag/AgCl was measured to be 0.69 V for DSDA-2TPA PI, 0.60 V for DSDA-2TPA-OMe₂ PI, and 0.75 V for DSDA-TPA-CN₂ PI. The $E_{1/2}$ for the external ferrocene/ferrocenium (F_c/F_{c+}) system was measured to be 0.57 V vs. Ag/AgCl in acetonitrile. Assuming that the HOMO level for the F_c/F_{c+} standard is –4.80 eV with respect to the zero vacuum level, the HOMO level was estimated to be –4.92 eV for DSDA-2TPA PI, –4.83 eV for DSDA-2TPA-OMe₂ PI, and –4.98 eV for DSDA-2TPA-CN₂ PI. From the measured band gap and HOMO level

data, the LUMO level was calculated to be –1.97 eV for DSDA-2TPA PI, –1.78 eV for DSDA-2TPA-OMe₂ PI, and –1.91 eV for DSDA-2TPA-CN₂ PI. These results indicate that the electron-donating methoxy substituent increased the HOMO level of the DSDA-2TPA PI, whereas the electron-accepting cyano substituent reduced the HOMO level. The tendency of the HOMO level is consistent with previous studies with conjugated polymers [24]. The band gap of DSDA-2TPA PI was somewhat increased by the methoxy and cyano substituents, leading to higher LUMO levels of the DSDA-2TPA-OMe₂ and DSDA-2TPA-CN₂ PIs.

The structures of the PIs in nanoscale thin films were examined by synchrotron GIXS analysis. The DSDA-2TPA PI film showed featureless 2D GISAXS pattern (Fig. 4A). Similar GISAXS patterns were observed for the other PIs in films (data not shown). These results indicate that no discernible nanostructure or microstructures were developed in all the PI films. In the 2D GIWAXS patterns, the PI films revealed only a broad, weak scattering ring like amorphous halo (Fig. 4a–c). The d -spacing of such scattering ring was determined to be 0.502 nm, regardless of the substituents. The scattering ring was attributed to the mean inter-chain distance of

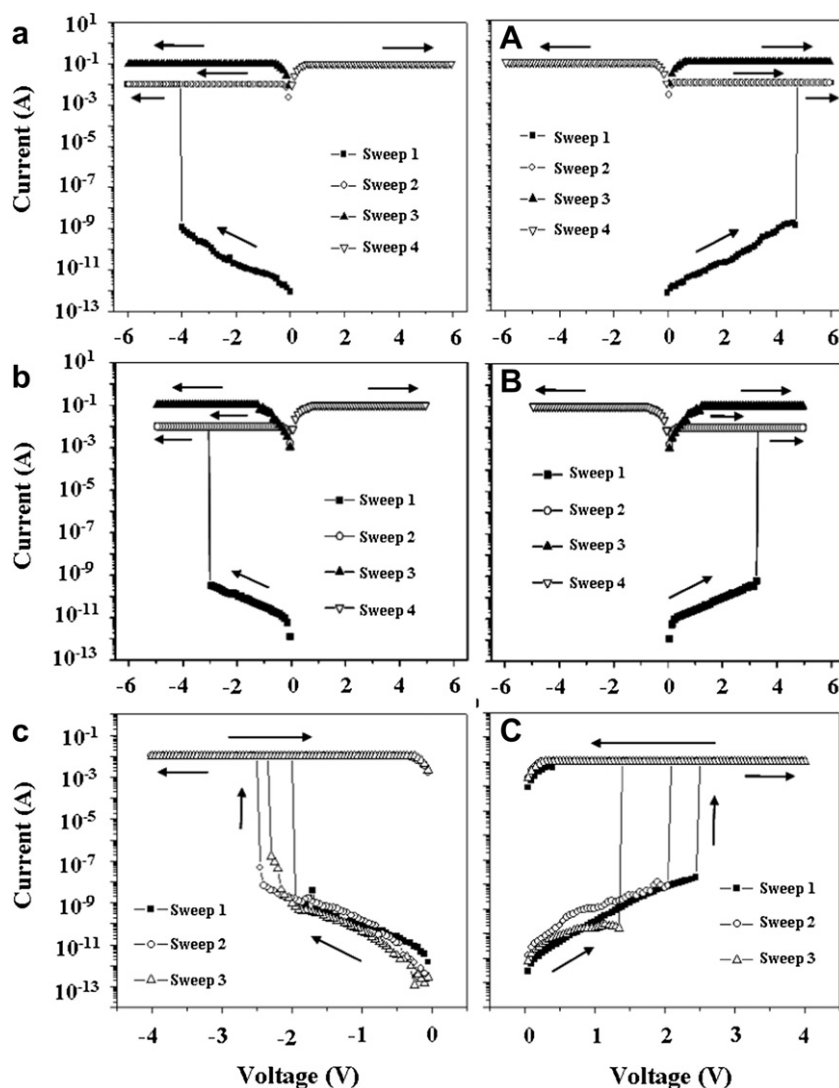


Fig. 6. Typical I–V curves of the Al/PI(30 nm thick)/Al devices, which were measured during voltage sweeps over the range from 0 to ± 6.0 V: (a,A) DSDA-2TPA PI; (b,B) DSDA-2TPA-OMe₂ PI; (c,C) DSDA-2TPA-CN₂ PI. In (a) and (A), as well as (b) and (B), the 1st and 2nd sweeps were conducted with a current compliance of 0.01 A while the 3rd and 4th sweeps were carried out with a current compliance of 0.1 A. In (c) and (C), the sweeps were performed with a current compliance of 0.01 A from 0 to –4.0 V or +4.0 V and back to 0 V (i.e. in dual sweep mode). The electrode contact area was 0.5×0.5 mm².

the PI polymer chains in the thin films. For all the PIs, the scattering ring was slightly anisotropic in intensity. Thus, an azimuthal scattering profile was extracted from each GIWAXS pattern along the amorphous halo ring. The obtained profiles were displayed in Fig. 4d as a function of azimuthal angle μ . For each PI film, the scattering intensity revealed a maximum at $\mu = 90^\circ$ and a minimum at $\mu = 0^\circ$ and 180° . Such anisotropy was in increasing order DSDA-2TPA PI < DSDA-2TPA-CN₂ PI < DSDA-2TPA-OMe₂ PI; in particular, the anisotropy was very weak for the DSDA-2TPA PI film. These results indicate that in the PI thin films, the polymer chains orient somewhat preferentially in the film plane rather than randomly.

In the memory devices, the PIs are in physical contact with the metal electrodes. Thus, the PI films in contact with the metal electrodes and the silicon substrates were further studied using synchrotron XR analysis. Representative XR profiles of the PI films are shown in Fig. 5a–c. All of the XR data were satisfactorily fitted using the Parratt algorithm [20,25]. The analysis results are summarized in Table 1. For the PI films deposited on the silicon substrates, the electron density ρ_e was 443.2 nm^{-3} for the DSDA-2TPA PI, 434.0 nm^{-3} for the DSDA-2TPA-OMe₂ PI, and 436.8 nm^{-3} for the DSDA-2TPA-CN₂ PI. These results indicated that the electron density of the DSDA-2TPA PI film was slightly reduced by the incorporations of methoxy and cyano substituents. The determined ρ_e values were reasonably consistent with values measured for PI films deposited on Al bottom and top electrodes. These results indicated that no aluminum atoms or ions diffused into the PI film layers during the deposition of the PI films on the Al bottom electrode. However, an interlayer with a thickness of 0.9–2.4 nm was detected for the PI films deposited on Al bottom electrodes. The thin interlayer was determined to have a root-mean-square (rms) roughness of 0.4–0.7 nm. The ρ_e values were determined to be in the range of 700.9 – 1109.3 nm^{-3} ; these ρ_e values are larger than that of aluminum. These results suggest that a thin aluminum oxide layer was formed on the Al bottom electrodes during the deposition of the PI films on the bottom electrodes. An interlayer was also determined to be present for the Al top electrodes deposited on the PI films. Its thickness ranged from 1.0 to 1.9 nm; these values were comparable to the surface roughnesses of the top electrodes. The ρ_e values were determined to be 407.7 – 530.5 nm^{-3} ; these values are closer to those of the PI films than that of aluminum or aluminum oxide. These results collectively indicated that no aluminum oxide was formed at the interface between the PI films and the Al top electrodes during the thermal deposition of the Al top electrodes in vacuum; if aluminum oxide was formed at this interface, it is likely that the amounts were low. Moreover, we combined the XR analysis data of the Al/PI and PI/Al samples together, producing a whole electron density profile of the Al/PI/Al devices as demonstrated in Fig. 5A–C.

With the above structure, interface and property details, devices were fabricated with the PI thin films (30 nm thick) and Al electrodes and their memory performance tested. All of the PI films initially exhibited a high resistance (OFF-state). However, when a positive or negative voltage was applied to the PI films, they exhibited an abrupt increase in the current over the range $+1.3$ – $+4.8 \text{ V}$, or -2.0 – -4.2 V (which corresponds to the critical voltage $V_{c,ON}$ to switch on the device) (Fig. 6). In devices, these OFF-to ON transitions can function as a “writing” process. After the devices reached their ON-state they showed various I–V characteristics, depending on the type of PI film. The DSDA-2TPA and DSDA-2TPA-OMe₂ PIs retained the ON-state even during reverse and forward voltage sweeps with a current compliance of 0.01 A or higher and even after the power was turned off (Fig. 6a and b and A and B). The ON/OFF current ratio was determined to be 10^6 – 10^{10} for the DSDA-2TPA film and 10^8 – 10^{10} for the DSDA-2TPA-OMe₂ film,

depending on the reading voltage. These results collectively informed that the DSDA-2TPA and DSDA-2TPA-OMe₂ PI films in the devices showed excellent WORM memory (i.e., permanent data storage) behavior without polarity. In case of the DSDA-2TPA-CN₂ PI, the ON-state retained during reverse and forward voltage sweeps but transformed to the OFF-state when the power was turned off. Namely, the DSDA-2TPA-CN₂ PI film exhibited DRAM behavior rather than WORM memory behavior. Such DRAM behavior was observed in both negative and positive voltage sweeps (Fig. 6c and C). The ON/OFF current ratio was determined to be 10^6 – 10^{10} , depending on the reading voltage.

Fig. 7 shows representative results of the stability tests for the ON- and OFF-state (namely, retention tests), which were carried out on the PI devices at room temperature in ambient conditions. The DSDA-2TPA PI film was switched to the ON-state by applying a voltage of $+4.8 \text{ V}$, whereas the DSDA-2TPA-OMe₂ PI film was switched to the ON-state by applying a voltage of $+3.5 \text{ V}$. For the DSDA-2TPA-CN₂ PI film, the ON-state was retained with continuous voltage bias of $+3.0 \text{ V}$. The ON- and OFF-states of all the PI films were retained without any degradation for a test period of 10 h. Overall, all the devices exhibited excellent reliability, even in ambient conditions.

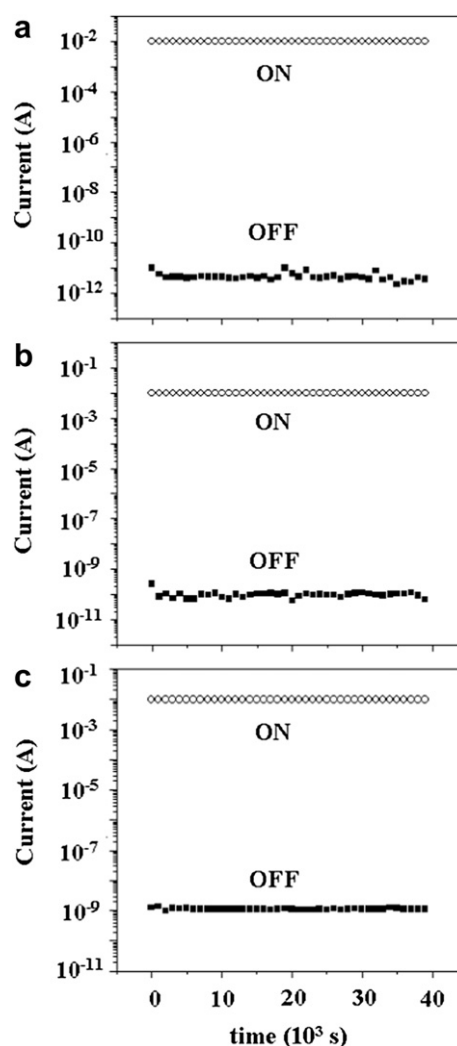


Fig. 7. Retention times of the ON- and OFF-states of the Al/PI (30 nm thick)/Al device: (a) DSDA-2TPA PI; (b) DSDA-2TPA-OMe₂ PI; (c) DSDA-2TPA-CN₂ PI. A reading voltage of $+0.5 \text{ V}$ was used for the ON-states of DSDA-2TPA and DSDA-2TPA-OMe₂ PIs, whereas a voltage of $+3.0 \text{ V}$ was employed for the ON-state of the DSDA-2TPA-CN₂ PI.

To investigate the electrical switching characteristics of the PI films in the devices, the measured I – V data were further analyzed in detail, using various conduction models [26–28]. The trap-limited space-charge limited conduction (SCLC) model was found to fit the I – V data for the OFF-state the best (Fig. 8a–c), while the Ohmic contact model was found to satisfactorily fit the I – V data for the ON-state (Fig. 8A–C). This showed that when the devices were in the OFF-state, a trap-limited SCLC mechanism was dominant, but when the devices were in the ON-state, Ohmic conduction was dominant. Moreover, the current levels in the devices in the ON-state were found to be independent of the device cell size, which is indicative of heterogeneous localized filament formation.

For the active PI film layers, the charge trapping sites might have arisen because of the chemical composition of the PIs. For all of the PIs, the 2TPA units are composed of two TPAs linked in a conjugation manner where TPA is an electron-donating group and thus known as a hole-transporting group. Thus, the 2TPA units can act as an electron-donating group. The imide carbonyl oxygens and sulfonyl oxygens are negatively polarized in part because of their relatively higher electronegativity against the carbonyl carbon. In contrast, the imide carbonyl carbons and sulfonyl sulfurs are positively polarized in part because of their relatively lower electronegativity against the carbonyl and sulfonyl oxygens. In addition, the DSDA-2TPA-OMe₂ PI had two additional methoxy substituents per 2TPA unit, which are known as an electron-

donating group, whereas the DSDA-2TPA-CN₂ PI had two additional cyano substituents per 2TPA unit, which are an electron-withdrawing group. All of these electron-donating and withdrawing groups and partially polarized imide ring and sulfonyl components are likely to have acted as charge-trapping sites. When a voltage is applied, filaments are formed in the PI films by such trap sites; their response to the current flow results mainly from the hopping of charges between the traps localized in the intra- and inter-molecular PI chains in the conduction paths (i.e., in the filaments).

For the devices with Al electrodes (whose work function ϕ is -4.28 eV) used in our study, the energy barrier for hole injection from the electrode to the active PI film layer (HOMO level) was estimated to be 0.64 eV for the DSDA-2TPA PI, 0.55 eV for the DSDA-2TPA-OMe₂ PI, and 0.70 eV for the DSDA-2TPA-CN₂ PI. The energy barrier for electron injection from the electrode to the active PI film layer (LUMO level) was estimated to be 2.31 eV for the DSDA-2TPA PI, 2.50 eV for the DSDA-2TPA-OMe₂ PI, and 1.80 eV for the DSDA-2TPA-CN₂ PI. All of the PI films showed a lower energy barrier for hole injection than for electron injection. These results therefore suggest that the conduction processes in the PI-based devices were dominated by hole injection. In increasing order, the energy barriers for hole injection in the films were DSDA-2TPA-OMe₂ PI < DSDA-2TPA PI < DSDA-2TPA-CN₂ PI. One might therefore expect that the critical switching-ON voltage $V_{c,ON}$ values would be

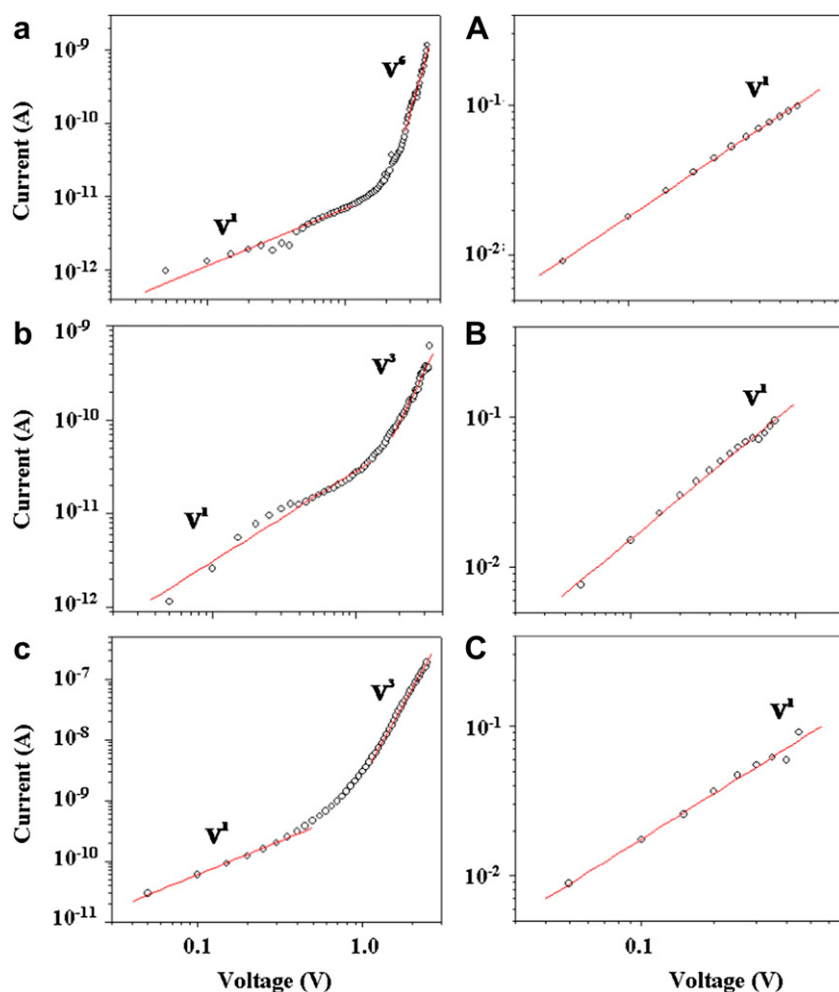


Fig. 8. Experimental (symbols) and fitted (solid lines) I – V curves for the Al/PI (30 nm thick)/Al devices: (a,A) DSDA-2TPA PI; (b,B) DSDA-2TPA-OMe₂ PI; (c,C) DSDA-2TPA-CN₂ PI. (a–c) OFF-state with the Ohmic (below 0.4–1.0 V) and the trap-limited SCLC (above 1.0 V) conduction model; (A–C) ON-state with the Ohmic current model.

in the increasing order DSDA-2TPA-OMe₂ PI < DSDA-2TPA PI < DSDA-2TPA-CN₂ PI. However, the $V_{C,ON}$ was observed to be in increasing order DSDA-2TPA-CN₂ PI < DSDA-2TPA-OMe₂ PI < DSDA-2TPA PI. Overall, the $V_{C,ON}$ of DSDA-2TPA PI was reduced by the incorporations of electron-donating methoxy group and electron-accepting cyano group, regardless of the differences in the energy barriers for hole injection.

As described above, interestingly the PIs in the devices demonstrated WORM memory or DRAM behavior, depending on the substituents of the 2TPA units. The DSDA-2TPA PI exhibited unipolar WORM memory behavior. The DSDA-2TPA-OMe₂ PI also showed similar WORM memory behavior although it had two additional electron-donating methoxy substituents per repeat unit and, however, its $V_{C,ON}$ was relatively lower than that of the DSDA-2TPA PI. These results suggest that the methoxy substituents did not significantly influence the memory behavior of DSDA-2TPA PI. Furthermore, the results inform that the incorporated methoxy substituents did not play well as charge-trapping sites. In contrast, the DSDA-2TPA-CN₂ PI revealed unipolar DRAM behavior, which is far different from the memory behavior of DSDA-2TPA PI. This can be attributed to at least two factors arising from the incorporation of the cyano substituents. First, the incorporated cyano substituents play a role as charging sites, in addition to the 2TPA, imide carbonyl, and sulfonyl units discussed above. Second, the cyano substituents are an electron-accepting group, and thus can reduce the electron-donating power of the 2TPA units. Overall, these factors of the cyano substituents act cooperatively to alter significantly the memory behavior of DSDA-2TPA PI.

4. Conclusions

Three aromatic PIs based on 2TPA derivatives with electron-donating and accepting substituents were synthesized, with reasonably high molecular weights: DSDA-2TPA, DSDA-2TPA-OMe₂, and DSDA-2TPA-CN₂ PIs. These polymers showed high thermal and dimensional stabilities compared with conventional aromatic PIs. The polymers produced high-quality nanoscale thin films with a smooth surface when they were applied in a conventional solution coating process. All of the PIs in the films were found to be amorphous, but they were oriented somewhat preferentially in the film plane, rather than randomly. Their film densities (i.e., electron density) and interchain distances were measured, and the HOMO and LUMO levels were determined.

In the Al/PI/Al devices, all of the PIs initially exhibited a high resistance (OFF-state). Under positive and negative voltage sweeps, the PIs demonstrated volatile or nonvolatile digital memory behavior, depending on the substituents of the 2TPA unit. The DSDA-2TPA and DSDA-2TPA-OMe₂ PI showed unipolar WORM memory behavior, whereas the DSDA-2TPA-CN₂ PI showed unipolar DRAM behavior. All of the PI films revealed excellent retention abilities in both the OFF- and ON-state, even under ambient air conditions. They also exhibited high ON/OFF current ratios (10^6 – 10^{10}). All of the memory behaviors were found to be governed by a mechanism involving trap-limited SCLC conduction and local filament formation. Moreover, all of the PI films showed a lower energy barrier for hole injection than for electron injection, suggesting that the conduction processes in the devices were dominated by hole injection.

The WORM memory characteristics of the DSDA-2TPA PI might have originated from the 2TPA, sulfonyl, and imide units in the polymer backbone, which acted as charge-trapping sites. Such WORM memory behavior was not significantly influenced by the addition of methoxy substituents, suggesting that the methoxy groups had a relatively low affinity for holes, and thus could not

perform well as charge-trapping sites. In contrast, such WORM memory behavior was found to be significantly affected by the incorporation of cyano substituents, confirming that the electron-accepting cyano groups could also act effectively as charge-trapping sites.

The methoxy and cyano substituents were further found to influence the HOMO and LUMO levels of the DSDA-2TPA PI; the energy barrier for charge injection in this PI varied depending on the substituents. Overall, the $V_{C,ON}$ of DSDA-2TPA PI was reduced by the incorporations of electron-donating methoxy group and electron-accepting cyano group, regardless of the differences in the energy barriers for hole injection.

Overall, this study has demonstrated that thermally, dimensionally stable DSDA-2TPA PI derivatives are highly suitable active materials for the low-cost mass production of high performance, polarity-free digital memory devices that can be operated with very low power consumption, high ON/OFF current ratios, and high thermal and dimensional stability. Moreover, the memory mode can be tuned by changing the substituent in the 2TPA unit.

Acknowledgments

This study was supported by the National Research Foundation (NRF) of Korea (Doyak Program (2011-0028678) and Center for Electro-Photo Behaviors in Advanced Molecular Systems (2010-0001784)) and by the Ministry of Education, Science & Technology (MEST), Korea (BK21 Program and World Class University Program (R31-2008-000-10059-0)). This work was also supported by the National Science Council of Taiwan, the Republic of China (NSC 98-2113-M-002-005-MY3). Synchrotron GIXS and XR measurements were supported by MEST, POSCO and POSTECH Foundation.

References

- [1] (a) Pinnow CU, Mikolajick T. *J Electrochem Soc* 2004;151:K13; (b) Donhauser Z, Mantooth B, Kelly K, Bumm L, Monnell J, Stapleton J, et al. *Science* 2001;292:2303; (c) Yang Y, Ouyang J, Ma L, Tseng RJH, Chu CW. *Adv Funct Mater* 2006;16:1011; (d) Baek S, Lee D, Kim J, Hong SH, Kim O, Ree M. *Adv Funct Mater* 2007;17:2637.
- [2] (a) Scott JC, Bozano LD. *Adv Mater* 2007;19:1452; (b) Ma D, Aguiar M, Freire JA, Hümmelgen IA. *Adv Mater* 2000;12:1063; (c) Henisch H, Meyers J, Callarotti R, Schmidt P. *Thin Solid Films* 1978;51:265; (d) Ling Q, Song Y, Ding SJ, Zhu C, Chan DSH, Kwong DL, et al. *Adv Mater* 2005;17:455.
- [3] (a) Lee TJ, Park S, Hahm SG, Kim DM, Kim K, Kim J, et al. *J Phys Chem C* 2009;113:3855; (b) Park S, Lee TJ, Kim DM, Kim JC, Kim K, Kwon W, et al. *J Phys Chem B* 2010;114:10294.
- [4] (a) Smits JHA, Meskers SCJ, Janssen RAJ, Marsman AW, de Leeuw DM. *Adv Mater* 2005;17:1169; (b) Choi S, Hong SH, Cho SH, Park S, Park SM, Kim O, et al. *Adv Mater* 2008;20:1766; (c) Lee D, Baek S, Ree M, Kim O. *IEEE Electron Device Lett* 2008;29:694; (d) Kim J, Cho S, Choi S, Baek S, Lee D, Kim O, et al. *Langmuir* 2007;23:9024.
- [5] (a) Hong SH, Kim O, Choi S, Ree M. *Appl Phys Lett* 2007;91:093517; (b) Lee D, Baek S, Ree M, Kim O. *Jpn J Appl Phys* 2008;47:5665; (c) Lee D, Baek S, Ree M, Kim O. *Electronics Lett* 2008;44:596.
- [6] (a) Deutsch A, Swaminathan M, Ree M, Surovic CW, Arjavalingam G, Prasad K, et al. *IEEE Trans Comp Packag Manuf Technol Part B Adv Packag* 1994;17:486; (b) Czornyj G, Chen K, Prada-Silva G, Arnold A, Souleotis K, Kim S, et al. *IEEE Electron Compon Tech Conf* 1992;42:682.
- [7] (a) Shin TJ, Ree M. *J Phys Chem B* 2007;111:13894; (b) Hahm SG, Lee SW, Suh J, Chae B, Kim SB, Lee SJ, et al. *High Perform Polym* 2006;18:549; (c) Ree M. *Macromol Res* 2006;14:1; (d) Ree M, Shin TJ, Lee SW. *Korea Polym J* 2001;9:1; (e) Wakita J, Jin S, Shin TJ, Ree M, Ando S. *Macromolecules* 2010;43:1930.
- [8] (a) Hahm SG, Lee TJ, Ree M. *Adv Funct Mater* 2007;17:1359; (b) Hahm SG, Lee TJ, Chang T, Jung JC, Zin WC, Ree M. *Macromolecules* 2006;39:5385; (c) Hahm SG, Lee SW, Lee TJ, Cho SA, Chae B, Jung YM, et al. *J Phys Chem B* 2008;112:4900;

- (d) Shin TJ, Ree M. *Langmuir* 2005;21:6081;
(e) Lee SW, Lee SJ, Hahm SG, Lee TJ, Lee B, Chae B, et al. *Macromolecules* 2005;38:4331;
(f) Kim Y, Goh WH, Chang T, Ha CS, Ree M. *Adv Eng Mater* 2004;6:39.
- [9] (a) Lee SW, Kim SI, Lee B, Kim HC, Chang T, Ree M. *Langmuir* 2003;19:10381;
(b) Chae B, Lee SW, Lee B, Choi W, Kim SB, Jung YM, et al. *J Phys Chem B* 2003;107:11911;
(c) Chae B, Lee SW, Lee B, Choi W, Kim SB, Jung YM, et al. *Langmuir* 2003;19:9459;
(d) Lee SW, Kim SI, Lee B, Choi W, Chae B, Kim SB, et al. *Macromolecules* 2003;36:6527;
(e) Lee SW, Chae B, Lee B, Choi W, Kim SB, Kim SI, et al. *Chem Mater* 2003;15:3105.
- [10] (a) Shin T, Park H, Lee S, Lee B, Oh W, Kim JS, et al. *Polym Eng Sci* 2003;43:1232;
(b) Chae B, Kim SB, Lee SW, Kim SI, Choi W, Lee B, et al. *Macromolecules* 2002;35:10119;
(c) Shin TJ, Ree M. *Macromol Chem Phys* 2002;203:791;
(d) Shin TJ, Lee B, Youn HS, Lee KB, Ree M. *Langmuir* 2001;17:7842;
(e) Lee SW, Chang T, Ree M. *Macromol Rapid Commun* 2001;22:941.
- [11] Ling QD, Chang FC, Song Y, Zhu CX, Liaw DJ, Chan DSH, et al. *J Am Chem Soc* 2006;128:8732.
- [12] Kim DM, Park S, Lee TJ, Hahm SG, Kim K, Kim JC, et al. *Langmuir* 2009;25:11713.
- [13] Lee TJ, Chang CW, Hahm SG, Kim K, Park S, Kim DM, et al. *Nanotechnology* 2009;20:135204.
- [14] Kim K, Park S, Hahm SG, Lee TJ, Kim DM, Kim JC, et al. *J Phys Chem B* 2009;113:9143.
- [15] Hahm SG, Choi S, Hong SH, Lee TJ, Park S, Kim DM, et al. *J Mater Chem* 2009;19:2207.
- [16] Hahm SG, Choi S, Hong SH, Lee TJ, Park S, Kim DM, et al. *Adv Funct Mater* 2008;18:3276.
- [17] Park S, Kim K, Kim JC, Kwon W, Kim DM, Ree M. *Polymer* 2011;52:2170.
- [18] Park S, Kim K, Kim DM, Kwon W, Choi J, Ree M. *ACS Appl Mater Interfaces* 2011;3:765.
- [19] (a) Cheng SH, Hsiao SH, Su TH, Liou GS. *Macromolecules* 2005;38:307;
(b) Chang CW, Yen HJ, Huang KY, Yeh JM, Liou GS. *J Polym Sci Part A Polym Chem* 2008;46:7937.
- [20] (a) Bolze J, Ree M, Youn HS, Chu SH, Char K. *Langmuir* 2001;17:6683;
(b) Hwang Y, Heo K, Chang CH, Joo MK, Ree M. *Thin Solid Films* 2006;510:159.
- [21] Salah F, Harzallah B, van der Lee AJ. *Appl Crystallogr* 2007;40:813.
- [22] (a) Yoon J, Kim KW, Kim J, Heo K, Jin KS, Jin S, et al. *Macromol Res* 2008;16:575;
(b) Lee B, Park YH, Hwang YT, Oh W, Yoon J, Ree M. *Nat Mater* 2005;4:147;
(c) Lee B, Oh W, Hwang Y, Park YH, Yoon J, Jin K, et al. *Adv Mater* 2005;17:696.
- [23] (a) Yoon J, Jin KS, Kim HC, Kim G, Heo K, Jin S, et al. *J Appl Crystallogr* 2007;40:476;
(b) Yoon J, Lee SW, Choi S, Heo K, Jin KS, Jin S, et al. *J Phys Chem B* 2008;112:5338;
(c) Kim G, Park S, Jung J, Heo K, Yoon J, Kim H, et al. *Adv Funct Mater* 2009;19:1631.
- [24] (a) Low PJ, Paterson MAJ, Yufit DS, Howard JAK, Cherryman JC, Tackley DR, et al. *J Mater Chem* 2005;15:2304;
(b) Zacharias P, Gather MC, Rojahn M, Nuyken O, Meerholz K. *Angew Chem Int Ed* 2007;46:4388.
- [25] Parratt LG. *Phys Rev* 1954;95:359.
- [26] (a) Mark P, Helfrich W. *J Appl Phys* 1962;33:205;
(b) Lampert MA. *Phys Rev* 1956;103:1648.
- [27] Campbell A, Bradley D, Lidzey D. *J Appl Phys* 1997;82:6326.
- [28] (a) Jensen KL. *J Vac Sci Technol B* 2003;21:1528;
(b) Frenkel J. *Phys Rev* 1938;54:647;
(c) Laurent C, Kay E, Souag N. *J Appl Phys* 1988;64:336.